

Time-Resolved SAXS Studies of the Kinetics of Thermally Triggered Release of Encapsulated Silica Nanoparticles from Block Copolymer Vesicles

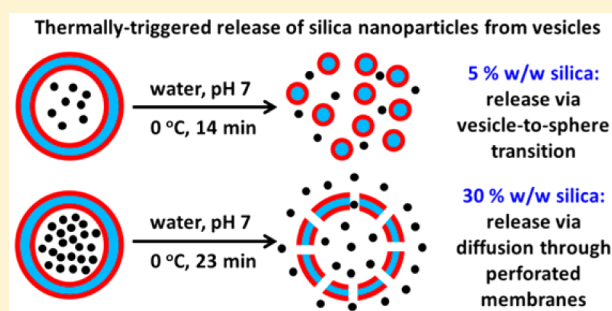
Charlotte J. Mable,[†] Matthew J. Derry,[†] Kate L. Thompson,[†] Lee A. Fielding,[‡] Oleksandr O. Mykhaylyk,^{*,†} and Steven P. Armes^{*,†}

[†]Department of Chemistry, University of Sheffield, Brook Hill, Sheffield S3 7HF, U.K.

[‡]The School of Materials, University of Manchester, Oxford Road, Manchester M13 9PL, U.K.

Supporting Information

ABSTRACT: Silica-loaded poly(glycerol monomethacrylate)-poly(2-hydroxypropyl methacrylate) diblock copolymer vesicles are prepared in the form of concentrated aqueous dispersions via polymerization-induced self-assembly (PISA). As the concentration of silica nanoparticles present during the PISA synthesis is increased up to 35% w/w, higher degrees of encapsulation of this component within the vesicles can be achieved. After centrifugal purification to remove excess non-encapsulated silica nanoparticles, SAXS, DCP, and TGA analysis indicates encapsulation of up to hundreds of silica nanoparticles per vesicle. In the present study, the thermally triggered release of these encapsulated silica nanoparticles is examined by cooling to 0 °C for 30 min, which causes *in situ* vesicle dissociation. Transmission electron microscopy studies confirm the change in diblock copolymer morphology and also enable direct visualization of the released silica nanoparticles. Time-resolved small-angle X-ray scattering is used to quantify the extent of silica release over time. For an initial silica concentration of 5% w/w, cooling induces a vesicle-to-sphere transition with subsequent nanoparticle release. For higher silica concentrations (20 or 30% w/w) cooling only leads to perforation of the vesicle membranes, but silica nanoparticles are nevertheless released through the pores. For vesicles prepared in the presence of 30% w/w silica, the purified silica-loaded vesicles were cooled to 0 °C for 30 min, and SAXS patterns were collected every 15 s. A new SAXS model has been developed to determine both the mean volume fraction of encapsulated silica within the vesicles and the scattering length density. Satisfactory data fits to the experimental SAXS patterns were obtained using this model.



INTRODUCTION

Microencapsulation is important for various industrial sectors, including orally administered drugs,¹ agrochemicals,^{2,3} and laundry products.^{4,5} This approach enables the controlled release of active components and can also prevent premature deactivation of mutually incompatible reagents such as enzyme denaturation by bleach in liquid laundry formulations.⁶ In particular, liposomes⁷ and block copolymer vesicles^{8–16} (a.k.a. “polymersomes”) are some of the most widely used carriers evaluated for drug delivery applications.^{17–21} Such hollow nanoparticles can be loaded with water-soluble drugs,^{22–24} hydrophilic dyes,²⁵ oligonucleotides,^{24,26,27} enzymes,²⁸ antibodies,²⁹ or magnetic nanoparticles.³⁰ In another example, gold nanoparticles and a fluorescent probe (calcein) have been loaded within liposomes and subsequently released using near-infrared light.³¹ This radiation is absorbed by the gold nanoparticles and converted into heat: the local rise in temperature causes the liposomal bilayers to become leaky, which triggers release of the calcein (and the gold nanoparticles).

Over the past five years or so, polymerization-induced self-assembly (PISA) has become established as a powerful tool for the rational design and efficient synthesis of a wide range of diblock copolymer nano-objects in either aqueous or non-aqueous media.^{16,32–34} Of particular relevance to the present study, RAFT aqueous dispersion polymerization can be utilized to prepare diblock copolymer vesicles directly in water at copolymer concentrations of up to 25% w/v solids.^{35–39} Periodic sampling during such syntheses has confirmed a progressive evolution in copolymer morphology: transmission electron microscopy (TEM) studies reveal that the transformation of highly anisotropic worms into well-defined vesicles proceeds via a so-called “jellyfish” intermediate.³⁶

We recently reported the successful *in situ* encapsulation of silica nanoparticles within poly(glycerol monomethacrylate)-poly(2-hydroxypropyl methacrylate) (PGMA–PHPMA) di-

Received: March 4, 2017

Revised: May 17, 2017

Published: May 26, 2017

block copolymer vesicles prepared via PISA.⁴⁰ These vesicles were synthesized at 10% w/w solids in the presence of 0–35% w/w silica nanoparticles followed by extensive purification via six centrifugation–redispersion cycles. Small-angle X-ray scattering (SAXS), disk centrifuge photosedimentometry, and cryo-TEM studies confirmed successful silica encapsulation within the vesicle lumen.

Given their biocompatibility and commercial availability, silica nanoparticles constitute a useful model cargo. Moreover, their high electron contrast aids TEM studies, they scatter X-rays strongly which facilitates SAXS analysis, and their excellent thermal stability enables convenient quantification via thermogravimetric analysis. Furthermore, silica nanoparticles are potentially an “active” payload. Recently, Rose et al.⁴¹ reported that strong adhesion between a freshly cleaved hydrogel can be rapidly achieved at ambient temperature simply by spreading an aqueous droplet containing silica nanoparticles on one of the two surfaces of the cleaved gel prior to contact. This approach can also be used for biological tissues such as calf’s liver, which suggests potential biomedical applications. However, silica nanoparticles encapsulated within block copolymer vesicles must be first released to become available for such tissue repair. It is well-known that certain vesicles can undergo morphological transitions when exposed to an external stimulus such as temperature,^{42–44} light,⁴⁵ salt,^{46,47} or pH.^{11,13,44,48,49} Herein we use time-resolved SAXS to monitor the rate of release of silica nanoparticles encapsulated within PGMA–PHPMA diblock copolymer vesicles by utilizing a thermally triggered morphological transition. A remarkable range of physical behavior is observed depending on the initial concentration of silica nanoparticles within such vesicles.

■ EXPERIMENTAL DETAILS

Materials and Methods. *Materials.* All reagents were used as received unless otherwise stated. 4,4′-Azobis(4-cyanopentanoic acid) (ACVA) and 2-cyano-2-propyl dithiobenzoate (CPDB) were purchased from Sigma-Aldrich (UK). Ethanol and dichloromethane were purchased from Fisher Scientific (UK). Glycerol monomethacrylate (GMA; 99.8% purity; 0.06 mol % dimethacrylate impurity) was kindly donated by GEO Specialty Chemicals (Hythe, UK) and used without further purification. 2-Hydroxypropyl methacrylate (HPMA) was purchased from Alfa Aesar (UK) and contained 0.07 mol % dimethacrylate impurity, as judged by HPLC analysis. CD₃OD was purchased from Goss Scientific (UK). Bindzil colloidal silica (CC401; supplied as a 40% w/w aqueous dispersion; manufacturer’s nominal particle diameter = 12 nm) was kindly donated by AkzoNobel Pulp and Performance Chemicals AB (Bohus, Sweden). 2,2′-Azobis[2-(2-imidazolin-2-yl)propane] dihydrochloride (VA-044) was purchased from Wako Specialty Chemicals (Japan). Deionized water (pH 6.2; surface tension = 72.0 mN m⁻¹ at 20 °C) was obtained using an Elga Elgastat Option 3A water purifier.

Synthesis of Silica-Loaded G₅₈H₂₅₀ Diblock Copolymer Vesicles. Such syntheses were described in detail in our recent work.⁴⁰ The protocol used for a 20% w/w aqueous silica dispersion is representative and is described here. G₅₈ macro-CTA (0.200 g, 0.021 mmol), HPMA monomer (0.758 g, 5.26 mmol), CC401 silica sol (4.80 g, 40% w/w aqueous dispersion), and deionized water (3.84 g) were weighed into a sample vial and purged with N₂ for 20 min. ACVA was added (1.18 mg, 0.0042 mmol, CTA/ACVA molar ratio = 5.0) and purged with N₂ for a further 10 min prior to immersion in an oil bath set at 70 °C for 2 h. Finally, the HPMA polymerization was quenched by cooling to room temperature with subsequent exposure to air. The protocols used for the 0, 5, 10, and 30% w/w aqueous silica dispersion formulations are the same, except the relative amounts of silica sol and deionized water are varied (see Table S1 in the

Supporting Information). To remove excess, nonencapsulated silica nanoparticles, the vesicles were diluted from 10% w/w to 1.0% w/w prior to performing six centrifugation–redispersion cycles (9000 rpm for 20 min for each cycle).

Copolymer Characterization. *Dynamic Light Scattering (DLS).* Intensity-average hydrodynamic diameters were recorded for aqueous copolymer dispersions and determined using a Malvern Zetasizer NanoZS instrument. Dilute aqueous dispersions (0.10% w/w) were analyzed at 25 °C using disposable cuvettes, and all data were averaged over three consecutive runs to give the hydrodynamic diameter (D_h).

Transmission Electron Microscopy (TEM). As-synthesized copolymer dispersions were diluted at 25 °C to generate 0.10% w/w dispersions. Copper/palladium TEM grids (Agar Scientific, UK) were surface-coated in-house to produce a thin film of amorphous carbon. The grids were then plasma glow-discharged for 30 s to create a hydrophilic surface. Individual samples of aqueous copolymer dispersions (0.1% w/w, 12 μL) were adsorbed onto the freshly glow-discharged grids for 20 s and then blotted with filter paper to remove excess solution. To stain the copolymer dispersions, uranyl formate solution (0.75% w/v; 9 μL) solution was placed on the sample-loaded grid for 20 s and then carefully blotted to remove excess stain. The grids were then dried using a vacuum hose. Imaging was performed at 100 kV using a Phillips CM100 instrument equipped with a Gatan 1 K CCD camera.

Small-Angle X-ray Scattering (SAXS). SAXS patterns were recorded at a synchrotron (ESRF, station ID02, Grenoble, France). A monochromatic X-ray beam ($\lambda = 0.0995$ nm) and a 2D SAXS detector (Rayonix MX-170HS) were used for these experiments. A q range of 0.004–2.0 nm⁻¹ was used for measurements, where $q = (4\pi \sin \theta)/\lambda$ corresponds to the modulus of the scattering vector and θ is half of the scattering angle. For these time-resolved measurements, a glass capillary of 2 mm thickness was inserted into a heating stage (HFSX350-CAP, Linkam Scientific Instruments, Tadworth, UK). X-ray scattering data were reduced (integration, normalization, and background subtraction) using standard routines available at the ID02 beamline. The scattering intensity of water was used for absolute scale calibration of the X-ray scattering patterns. Irena SAS macros⁵⁰ for Igor Pro were utilized for modeling and further SAXS analysis. Copolymer vesicle dispersions were diluted from 10% w/w (as-synthesized) to 1.0% w/w and then subjected to six centrifugation–redispersion cycles prior to data collection. For time-resolved studies, dilute aqueous dispersions were cooled to 0 °C for 30 min with SAXS patterns being collected every 15 s.

■ RESULTS

For the sake of brevity, a shorthand notation is utilized throughout this article to describe the copolymer. Thus, G₅₈H₂₅₀ represents a PGMA–PHPMA diblock copolymer, where 58 and 250 indicate the mean degrees of polymerization (DP) of the two respective blocks.

The thermoresponsive behavior of 1.0% w/w copolymer dispersions of both empty and silica-loaded G₅₈H₂₅₀ vesicles (originally prepared via PISA at 10% w/w copolymer in the presence of either 5, 10, 20, or 30% w/w silica nanoparticles, followed by purification via multiple centrifugation–redispersion cycles to remove excess free silica) was examined by cooling to approximately 0 °C using an ice bath. The initial vesicle dispersions were turbid at room temperature, as expected. After cooling for 30 min, the samples prepared in the presence of either 0 or 5.0% w/w silica were no longer turbid, whereas those prepared using 10, 20, and 30% w/w silica remained turbid.

TEM images and dynamic light scattering (DLS) studies indicated that the empty and silica-loaded G₅₈H₂₅₀ vesicles each had a mean hydrodynamic diameter (D_h) of approximately 390 nm at 25 °C (see Figure 1). However, when the empty vesicles were cooled in ice for 30 min, spheres were obtained with a D_h

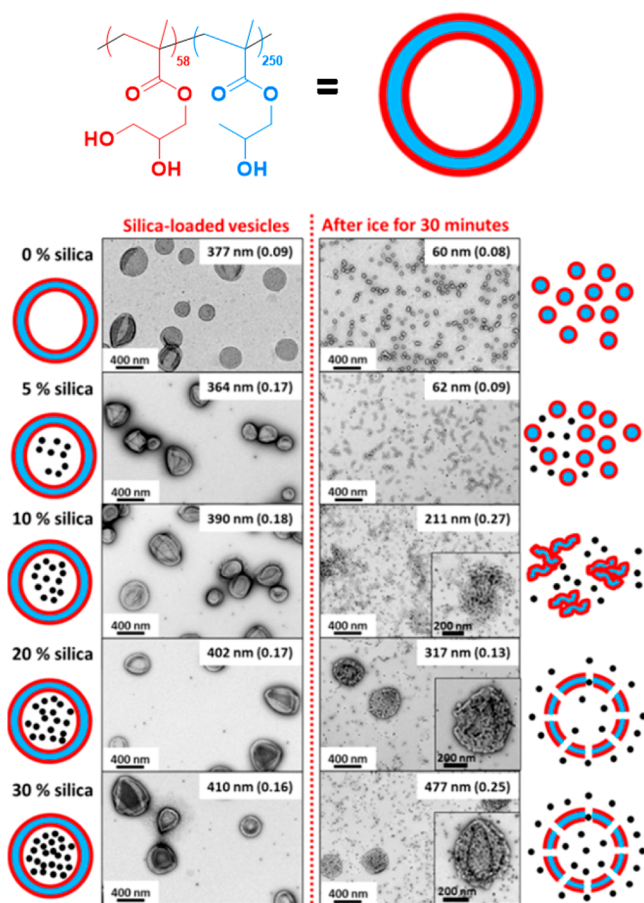


Figure 1. Chemical structure of PGMA₅₈-PPHMA₂₅₀ diblock copolymer, TEM images and schematic cartoons of silica-loaded G₅₈H₂₅₀ diblock copolymer vesicles synthesized in the presence of varying amounts of silica nanoparticles (0–30% w/w silica) after six centrifugation–redispersion cycles to remove excess silica, before (left) and after (right) being held in ice for 30 min. Dynamic light scattering hydrodynamic diameters and associated polydispersities are stated in the inset of each TEM image.

of 60 nm (see Figure 1). This morphological transition was expected because a mean degree of polymerization of 250 was targeted for the structure-directing PHPMA block so as to produce vesicles that lie close to the worm–vesicle phase boundary.⁴⁴ Cooling leads to greater surface plasticization of the PHPMA membranes, which results in a thermally triggered morphological transition to produce either worms or spheres.

Similar observations were made for the silica-loaded G₅₈H₂₅₀ diblock copolymer vesicles synthesized in the presence of 5.0% w/w silica nanoparticles. After cooling to 0 °C for 30 min, a mixture of pseudo-spherical copolymer nanoparticles and free silica nanoparticles can be observed by TEM (see Figure 1). Moreover, the D_h is reduced from 364 nm at 25 °C to 62 nm after 30 min at 0 °C. These results confirm that the silica-loaded vesicles dissociate to form spheres under these conditions, thus releasing the encapsulated silica nanoparticles.

For the silica-loaded G₅₈H₂₅₀ vesicles synthesized in the presence of 10% w/w silica, worm-like aggregates and free silica nanoparticles are observed by TEM after 30 min at 0 °C (see Figure 1). Furthermore, for silica-loaded G₅₈H₂₅₀ vesicles synthesized in the presence of 20 or 30% w/w silica, TEM analysis suggests that at least some of the vesicles remain intact, despite apparent release of the encapsulated silica nanoparticles

(see Figure 1). In both cases, DLS studies indicate little change in D_h. However, close inspection reveals that the remaining vesicles after cooling to 0 °C for 30 min appear to have perforated membranes (see cartoon in Figure 1). Prior to this study, we did not anticipate that the encapsulated silica payload might affect the thermally triggered morphological transition because the vesicles comprise the same G₅₈H₂₅₀ copolymer composition in all cases. However, both TEM images and DLS studies indicate that increasing the silica payload leads to qualitatively different thermoresponsive behavior.

Both Derry et al.⁵¹ and Förster and co-workers⁵² have recently reported that time-resolved SAXS can be used to monitor changes in block copolymer morphology over time. Thus, in order to gain a better understanding of the silica release mechanism(s), time-resolved SAXS studies were conducted on the G₅₈H₂₅₀ vesicles prepared via PISA at 10% w/w copolymer in the presence of either 0, 5, or 30% w/w silica nanoparticles. If required, these dispersions were purified to remove excess silica via multiple centrifugation–redispersion cycles, then diluted to 1.0% w/w copolymer, and cooled to 0 °C for 30 min while recording SAXS patterns at 15 s intervals.

SAXS patterns obtained for the empty G₅₈H₂₅₀ vesicles suggest that they remained intact for up to 5 min at 0 °C. Selected SAXS patterns (recorded after 0, 2.5, and 5 min) were fitted using a vesicle model,⁵³ which provided satisfactory data fits (see Figure 2). The radius from the center of the vesicle to

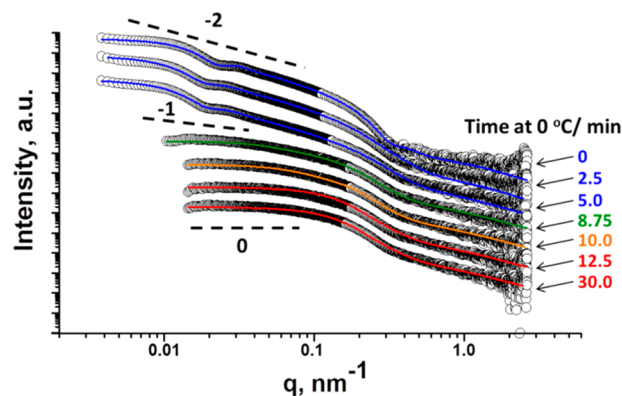


Figure 2. SAXS patterns obtained for 1.0% w/w aqueous dispersions of G₅₈H₂₅₀ vesicles (originally prepared via PISA at 10% w/w copolymer in the absence of 18.4 nm silica nanoparticles). The G₅₈H₂₅₀ vesicles were cooled to 0 °C for 30 min with scattering patterns being recorded at 15 s intervals. Selected SAXS patterns recorded after various times at 0 °C are shown (for clarity, these patterns are shifted vertically by an arbitrary scaling factor). Owing to the relatively high signal/noise ratio, patterns recorded from 8.75 to 30 min were truncated at low q . Black open circles show the experimental data, and data fits are indicated by solid lines. Vesicles are present at 0 °C for up to 5 min (blue fits) but subsequently undergo dissociation to form worm-like micelles after 8.75 min (green fit), followed by formation of spherical micelle dimers after 10 min (orange fit) and spheres after 12.5 min (red fits).

the center of the membrane, R_m , remained relatively constant, while the mean vesicle membrane thickness, T_m , was reduced from 15.9 ± 2.5 to 10.9 ± 3.6 nm over time at 0 °C. The volume fraction of water within the membrane, x_{sol} , increased from 0.16 to 0.69 after 5 min at 0 °C. This indicates greater hydration of the membrane-forming PHPMA block, as previously reported by Blanazs et al. for G₅₄H₁₄₀ worms at 4 °C.^{54,55} After 5 min, the highly plasticized vesicles begin to

dissociate: worms are formed after 8.75 min at 0 °C, as indicated by the gradient in the $I(q)$ vs q plot tending to negative unity at low q .⁵⁶ An established worm-like micelle model^{57–59} provided a reasonably good fit to the corresponding scattering pattern (see Figure 2; data set recorded after 8.75 min). The worm cross-section radius, R_{wcs} , was determined to be 9.0 ± 3.1 nm, with a mean worm contour length, L_w , of 349 nm and a worm Kuhn length, K_w , of 76.2 nm. The water volume fraction x_{sol} was determined to be 0.88 for the worms, which is significantly higher than that observed for the vesicles. Such vesicle-to-worm transitions are believed to be the result of *surface plasticization* of the membrane, which leads to an increase in the effective stabilizer block DP and hence a reduction in the packing parameter.⁴⁴ After 10 min at 0 °C, a spherical dimer model⁴³ produced a good fit to the SAXS pattern (Figure 2, 10 min), indicating worm dissociation according to the model proposed by Blanazs et al.⁵⁵ The worm core radius, R_s , and x_{sol} were determined to be 11.2 ± 4.2 nm and 0.89, respectively. The low q gradient tends to zero for all SAXS patterns collected after 12.5 min, indicating the formation of approximately spherical particles.⁵⁶ Hence a spherical micelle model^{57–60} was utilized to fit all SAXS patterns recorded over longer time scales. Data fits were consistent with the formation of spheres with a R_s of 14.6 ± 4.3 nm and an x_{sol} of 0.87.

It is perhaps worth noting that the spherical dimers formed after 10 min have a significantly smaller R_s value compared to that obtained for the spheres formed after 12.5 min (11.2 ± 4.2 nm vs 14.6 ± 4.3 nm, respectively). This significant increase in R_s when going from spherical dimers to spheres can be rationalized by considering the spatial redistribution of copolymer chains that occurs during this transition (see Figure S1). This explanation also applies to the preceding worm-to-dimer transition. In this latter case, the R_{wcs} for the worms formed after 8.75 min at 0 °C is 9.0 ± 3.1 nm, which is significantly smaller than that for the dimers formed after 10 min.

For the SAXS patterns recorded after 0, 8.75, and 30 min at 0 °C, data fits using appropriate models enabled the mean aggregation number (N_{agg}) for the vesicles, worms, and spheres to be determined using the following three equations:

$$N_{agg \text{ vesicle}} = (1 - x_{sol}) \frac{V_{out} - V_{in}}{V_{co}} \quad (1)$$

$$N_{agg \text{ worm}} = (1 - x_{sol}) \frac{\pi R_{wcs}^2 L_w}{V_{co}} \quad (2)$$

$$N_{agg \text{ sphere}} = (1 - x_{sol}) \frac{(4/3)\pi R_s^3}{V_{co}} \quad (3)$$

where $V_{out} = \frac{4}{3}\pi(R_m + \frac{1}{2}T_m)^3$, $V_{in} = \frac{4}{3}\pi(R_m - \frac{1}{2}T_m)^3$, and V_{co} is the volume of the hydrophobic PHPMA core-forming (or membrane-forming) block. Using the above three equations, we calculate approximately 49 900 copolymer chains per vesicle, 185 copolymer chains per worm, and 29 copolymer chains per sphere. Assuming that the main source of uncertainty arises from the standard deviation in the sphere radius, a conservative estimate for the uncertainty in the associated N_{agg} is approximately 32%. Significantly larger values are expected for the more polydisperse worms and vesicles. Nevertheless, the calculated N_{agg} values suggest that, on cooling to 0 °C, each

vesicle dissociates to form 270 worms and, ultimately, 1750 spheres (thus each worm comprises approximately 7 spheres).

SAXS patterns recorded for $G_{58}H_{250}$ vesicles synthesized in the presence of 5.0% w/w silica indicate that silica-loaded vesicles are initially present at 25 °C while spheres are formed after 30 min at 0 °C (see Figure 3). This vesicle-to-sphere

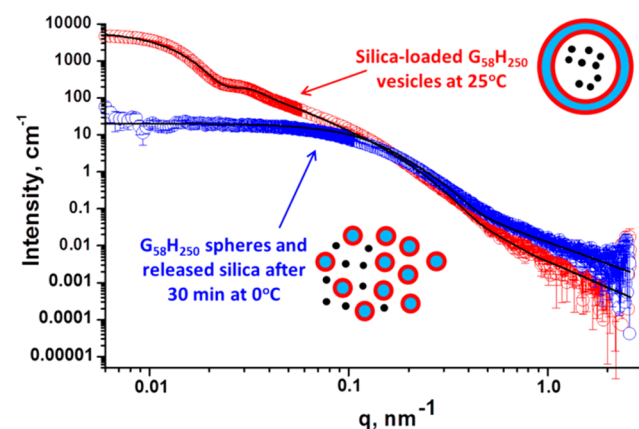


Figure 3. SAXS patterns obtained for a 1.0% w/w aqueous dispersion of purified silica-loaded $G_{58}H_{250}$ vesicles (originally prepared via PISA at 10% w/w copolymer in the presence of 5.0% w/w silica nanoparticles) at 25 °C (red data) and after cooling the same vesicles to 0 °C for 30 min (blue data). Solid black lines represent data fits in each case using a two-population SAXS model (see main text for details).

transition is accompanied by release of the encapsulated silica nanoparticles as confirmed by TEM studies (see Figure 1). Satisfactory fitting of the initial SAXS pattern recorded at 25 °C required a two-population “vesicle plus sphere” model (see Supporting Information for further details of this SAXS model).⁴⁰ The parameters used to represent the sphere component of this model were derived from SAXS studies of the pristine silica nanoparticles alone (Figure S5 and Table S2). According to its manufacturer (AkzoNobel), approximately 50% of the surface silanol groups on the CC401 silica nanoparticles are glycerol-functionalized. This means that such silica sols are significantly less charged than conventional aqueous silica sols yet still exhibit some anionic character. Thus, depending on the surface charge density and background salt, it might be necessary to account for electrostatic interactions between silica nanoparticles when modeling the SAXS data. In principle, this correction requires a suitable Hayter–Penfold structure factor for charged particles.⁶¹ However, SAXS studies of aqueous silica dispersions of varying concentration indicated that the well-known Percus–Yevick approximation⁶² for hard (uncharged) spheres produced satisfactory SAXS data fittings (Figure S5) and physically realistic particle dimensions and silica volume fractions (Table S2). Thus the Percus–Yevick model is considered to be a sufficiently good approximation for structural analysis of the silica-loaded vesicles to determine silica volume fractions from the SAXS data. The silica-loaded vesicles had a mean R_m of 127.8 ± 30.5 nm, a T_m of 15.4 ± 2.2 nm, and an x_{sol} of 0.16. However, a two-population “spherical micelle^{57–60} plus sphere” model was required to obtain a reasonably good fit to the SAXS pattern observed after 30 min at 0 °C. Some deviation in the data fit was observed at around $q \sim 0.1$ nm⁻¹, which is ascribed to minor populations of dimers and trimers.⁴³ Such species can be observed in the TEM image

shown in Figure 1. As expected, the silica nanoparticles were unaffected by lowering the temperature because the R_s for this component remained constant at 9.2 ± 2.1 nm. The $G_{58}H_{250}$ spheres formed after 30 min at 0°C exhibited an R_s of 14.6 ± 4.3 nm and an x_{sol} of 0.88, which are comparable values to those observed for the empty $G_{58}H_{250}$ vesicles. In summary, the

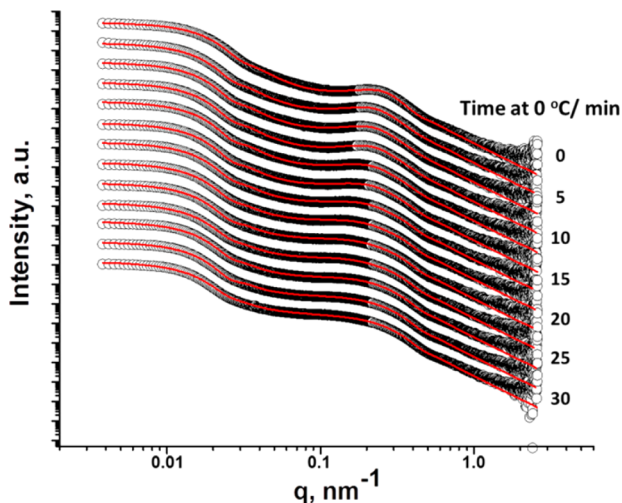


Figure 4. SAXS patterns obtained for a 1.0% w/w aqueous dispersion of $G_{58}H_{250}$ vesicles (originally prepared via PISA at 10% w/w copolymer in the presence of 30% w/w silica nanoparticles). Excess nonencapsulated silica nanoparticles were removed via six centrifugation–redispersion cycles. The resulting purified silica-loaded $G_{58}H_{250}$ vesicles were cooled to 0°C for 30 min while SAXS patterns were recorded at 15 s intervals. Only selected patterns recorded after various times at 0°C are shown (for clarity, these patterns are shifted vertically by an arbitrary scaling factor). The experimental data are represented by black open circles while solid red lines show the data fits calculated using a two-population “vesicle plus sphere” model.

thermally triggered morphological transition observed for the silica-loaded $G_{58}H_{250}$ vesicles prepared in the presence of 5.0% w/w silica nanoparticles is essentially identical to that found for the empty $G_{58}H_{250}$ vesicles.

In contrast, time-resolved SAXS patterns recorded for silica-loaded $G_{58}H_{250}$ vesicles prepared in the presence of 30% w/w silica nanoparticles indicate that the original vesicles remained intact after cooling to 0°C for 30 min (see Figure 4). These observations are also supported by TEM studies (see Figure 1). However, the structure factor peak at $q \sim 0.25\text{ nm}^{-1}$ corresponding to the relatively high local concentration of encapsulated silica nanoparticles gradually disappears over time. This is consistent with release of the encapsulated nanoparticles, since this leads to a reduction in the effective silica concentration.

Fitting the corresponding SAXS patterns requires a sophisticated model that accounts for both the $G_{58}H_{250}$ vesicles and the spherical silica nanoparticles (see Supporting Information for further information).⁴⁰ In order to study the extent of silica release under such conditions, this “vesicle plus sphere” two-population model was modified to include two new fitting parameters. For the vesicle model, the effective scattering length density of the lumen, ξ_{lum} , was included as a fitting parameter in order to assess the rate of silica release from the vesicles at 0°C . The scattering length density of pure amorphous silica, ξ_{SiO_2} , is $17.5 \times 10^{10}\text{ cm}^{-2}$, and that of water, $\xi_{\text{H}_2\text{O}}$, is $9.42 \times 10^{10}\text{ cm}^{-2}$. At 25°C , the vesicle lumen contains

both silica nanoparticles and water. Fitting the SAXS pattern of the original silica-loaded vesicles indicates that ξ_{lum} is $11.75 \times 10^{10}\text{ cm}^{-2}$. This value is intermediate between that of silica and water, as expected. The numerical value of ξ_{lum} is gradually reduced over time at 0°C (see Figure 5a and Table 1). For

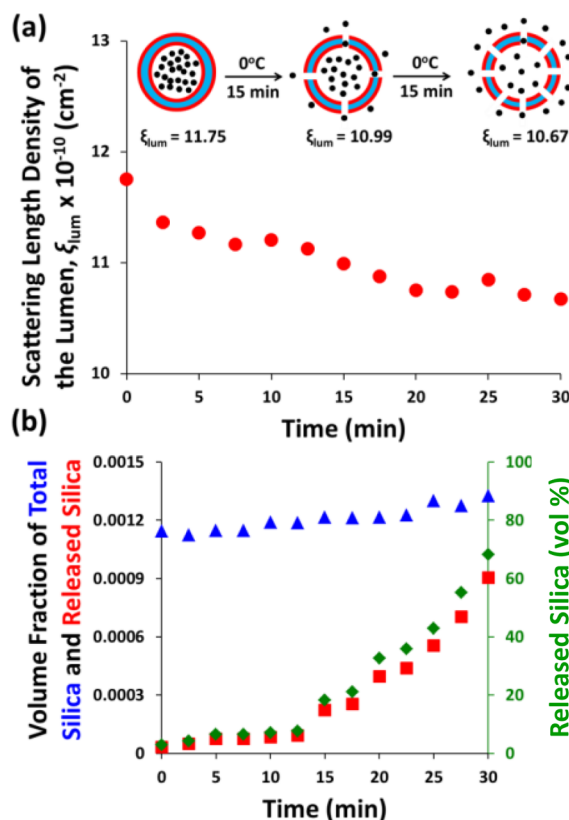


Figure 5. (a) Plot of the scattering length density of the $G_{58}H_{250}$ diblock copolymer vesicle lumen (ξ_{lum}) against time held at 0°C (red circles). Inset: schematic cartoon illustrating how the release of silica nanoparticles from inside the vesicles changes the ξ_{lum} as the purified silica-loaded vesicles (originally prepared via PISA at 10% w/w copolymer in the presence of 30% w/w silica) are cooled to 0°C for 30 min. (b) Plot of the total volume fraction of silica in the system (blue triangles corresponding to left-hand y-axis), the volume fraction of released silica (red squares corresponding to left-hand y-axis), and the amount of released silica (green diamonds corresponding to right-hand y-axis) against the time at which the purified silica-loaded $G_{58}H_{250}$ diblock copolymer vesicles (originally prepared with 30% w/w silica) were cooled at 0°C .

example, the ξ_{lum} decreased to $10.99 \times 10^{10}\text{ cm}^{-2}$ after 15 min at 0°C and to $10.67 \times 10^{10}\text{ cm}^{-2}$ after a further 15 min. This reduction in X-ray contrast for the lumen confirms that the encapsulated silica nanoparticles are gradually released from the vesicles over time. Furthermore, these data suggest that initially the vesicle lumen contains approximately 29 vol % silica (with the remaining volume being water), which is reduced to 15 vol % silica after 30 min at 0°C . This suggests that approximately 52% of the encapsulated silica nanoparticles are released under these conditions. However, the ξ_{lum} is an average over the entire lumen. It assumes that the silica nanoparticles (and hence the electrons) are uniformly distributed throughout the vesicle lumen, but in practice this may not be the case.

For the sphere model, two subpopulations are used to model the silica component for the release kinetics: the silica

Table 1. Summary of SAXS Structural Parameters Obtained for Diluted 1.0% w/w Aqueous Copolymer Dispersions of Purified G₅₈H₂₅₀ Vesicles (Originally Prepared via PISA at 10% w/w Copolymer in the Presence of 30% w/w Silica) When Cooled to 0 °C for 30 min^a

time/min	population 1 (vesicles) ^b		population 2 (silica nanoparticles) ^c			
	R _m (σ _{Rm})/nm	ξ _{lum}	C _{SiO₂}	C _{rel}	f _{PY}	R _{PY} /nm
0	141.0 (26.7)	11.75	0.00114	0.0000319	0.195	113
2.5	148.3 (33.3)	11.36	0.00112	0.0000477	0.175	127
5.0	149.9 (32.8)	11.26	0.00115	0.0000734	0.175	130
7.5	150.3 (32.7)	11.16	0.00115	0.0000736	0.177	132
10.0	150.9 (31.4)	11.20	0.00119	0.0000830	0.150	136
12.5	149.5 (31.7)	11.12	0.00119	0.0000908	0.131	134
15.0	149.1 (33.8)	10.99	0.00121	0.0002213	0.114	148
17.5	149.3 (34.0)	10.87	0.00121	0.0002547	0.086	158
20.0	149.8 (33.3)	10.75	0.00121	0.0003959	0.069	170
22.5	147.3 (36.2)	10.73	0.00123	0.0004388	0.063	181
25.0	149.0 (33.6)	10.85	0.00130	0.0005559	0.066	156
27.5	150.7 (33.3)	10.71	0.00127	0.0007022	0.048	161
30.0	146.7 (39.0)	10.67	0.00132	0.0009038	0.066	251

^aScattering patterns were recorded every 15 s. Selected SAXS patterns recorded after 2.5 min intervals at 0 °C were analyzed using a two-population model comprising vesicles and spheres, with the latter component representing the silica nanoparticles. Vesicle parameters for population 1 are as follows: R_m is the mean radius from the center of the vesicle to the center of the membrane, σ_{Rm} is the associated standard deviation, and ξ_{lum} is the scattering length density of the vesicle lumen. Sphere parameters for population 2 are as follows: C_{SiO₂} is the total volume fraction of silica nanoparticles in the aqueous dispersion, C_{rel} is the volume fraction of released silica nanoparticles, f_{PY} is the Percus–Yevick effective volume fraction of the packed silica spheres, and R_{PY} is the Percus–Yevick correlation radius of the packed spheres. ^bThe copolymer volume fraction in the dispersion (C_{copolymer}), the membrane thickness (T_m) and its associated standard deviation (σ_{Tm}), and the radius of gyration of the PGMA corona block (R_g) were each fixed at 0.001, 15.9, 2.2, and 2.3 nm, respectively. ^cThe core radius (R_{SiO₂}) and its associated standard deviation (σ_{RSiO₂}) were fixed at 9.2 and 2.1 nm, respectively.

nanoparticles released from the vesicles are described by a spherical form factor while the silica nanoparticles remaining within the vesicle lumen are described by a sphere model with a structure factor for interacting hard spheres. The relative contributions made to the overall scattering by these two subpopulations were used to determine the fraction of encapsulated silica nanoparticles at any given time interval (see Supporting Information, eq S10). The volume fraction of released silica, C_{rel}, was included as a fitting parameter.

C_{rel} increased from an initial value of 3.19 × 10⁻⁵ at 0 °C to 9.04 × 10⁻⁴ after 30 min at this temperature (see Figure S5b and Table 1). As expected, the overall silica volume fraction in the dispersion, C_{SiO₂}, remains essentially constant, which validates this analytical approach (see Figure S5b and Table 1). SAXS analysis indicates that 68% silica is released from the silica-loaded vesicles within 30 min at 0 °C. This is reasonably comparable to the release of 52% silica estimated by fitting ξ_{lum} under the same conditions.

As discussed above ξ_{lum} is averaged over the entire vesicle lumen, so the silica volume fraction obtained from the measurements of C_{rel} is considered to be more accurate. Furthermore, the Percus–Yevick correlation radius for densely packed spheres (R_{PY}) was initially 113 nm at 0 °C and 251 nm after 30 min at 0 °C (see Table 1). This suggests that the released silica nanoparticles become well-dispersed in the aqueous continuous phase after vesicle dissociation occurs. Moreover, the Percus–Yevick effective volume fraction for packed spheres, f_{PY}, is reduced from 0.195 to 0.066 (see Table 1), thus confirming partial release of the silica nanoparticles from the vesicle lumen.

In summary, the silica nanoparticles are initially relatively densely packed within the vesicles at 25 °C, which leads to a prominent structure factor, a high ξ_{lum}, a small C_{rel}, a short R_{PY},

and a large f_{PY}. After 30 min at 0 °C, a substantial fraction of the encapsulated silica nanoparticles are released from the slowly dissociating vesicles, leading to loss of the original structure factor, a lower ξ_{lum}, a larger C_{rel}, a larger R_{PY}, and a smaller f_{PY}.

DISCUSSION

One important question that arises from this study is the following: how do the encapsulated silica nanoparticles get released if the vesicles sometimes apparently remain intact? In principle, one plausible explanation is that the smaller vesicles dissociate preferentially compared to the larger vesicles because the former species have a higher radius of curvature. If such size-dependent dissociation occurred, the mean vesicle diameter should increase with aging time at 0 °C with a concomitant reduction in the vesicle number density. The latter parameter can be estimated using the X-ray scattering intensity at 0.01 nm⁻¹ and does indeed decrease approximately two-fold (from ~16 000 to ~7000 cm⁻¹; see Figure S2). However, the mean vesicle radius, R_m, remains relatively constant at ~149 nm for the G₅₈H₂₅₀ vesicles, regardless of their aging time at 0 °C (see Table 1). This suggests that vesicle dissociation is not in fact size-dependent.

An alternative explanation is that all vesicles, regardless of their size, eventually comprise perforated (and hence permeable) membranes while remaining intact, enabling silica nanoparticles to diffuse out through the increasingly porous membrane. As discussed above, TEM images suggest that the vesicles do indeed remain intact and there is also good evidence for membrane perforation. Moreover, close inspection suggests that the pore dimensions are comparable to the number-average diameter of the silica nanoparticles (estimated to be 13 ± 3 nm by measuring 100 nanoparticles). Hence, in principle,

the silica nanoparticles can escape from the vesicles if membrane perforation becomes extensive. However, this hypothesis does not explain the apparent reduction in vesicle number density indicated in the SAXS studies, unless this is actually an artifact related to membrane perforation.

Moreover, neither hypothesis explains why $G_{58}H_{250}$ vesicles readily dissociate to form spheres in the absence of any silica nanoparticles yet do not apparently undergo dissociation at all if they contain relatively high silica loadings. Thus, control experiments were performed to examine whether varying the silica nanoparticle concentration present in the continuous phase had any significant effect on the vesicle release kinetics or mechanism. Empty $G_{58}H_{250}$ vesicles prepared in the absence of any silica nanoparticles were added in turn to either a 5.0 or 30% w/w aqueous dispersion of silica nanoparticles. Each vesicle/silica binary mixture was then cooled to 0 °C for 30 min. TEM studies confirmed that the empty vesicles dissociated to form spheres, regardless of the background silica concentration (see Figure S3). Thus, the presence of silica in the aqueous continuous phase clearly does not confer additional vesicle stabilization.

According to a recent review article by Dimova, “the bending rigidity of membranes is a sensitive indicator for the presence of inclusions or adsorbing species”.⁶³ Thus, an intriguing question is whether the encapsulated silica nanoparticles can somehow reinforce the vesicle membrane. At first sight, this tentative explanation looks rather attractive because the silica-loaded vesicles certainly become significantly more stable than empty vesicles when subjected to the same thermal trigger. Furthermore, higher silica loadings enhance the vesicle membrane stability with respect to the thermally triggered release of such nanoparticles. In principle, the silica nanoparticles may physically adsorb to the inner surface of the vesicle lumen, which is likely to reinforce the vesicle morphology. However, there is no direct experimental evidence to support this hypothesis, either in the TEM images or in the SAXS data collected at 25 °C. [If silica nanoparticles did adsorb to the inner lumen, the most likely change in the SAXS pattern would be a more pronounced structure factor at intermediate q . Unfortunately, SAXS is not sufficiently sensitive to detect such local ordering.]

The silica nanoparticle concentration within the vesicles also affects the characteristic time scale required for the observed morphological transitions. The X-ray scattering intensity at $q \sim 0.01 \text{ nm}^{-1}$ was analyzed over time at 0 °C (see Figure S4). For the $G_{58}H_{250}$ vesicles prepared in the absence of any silica, the vesicle-to-sphere transition requires approximately 12 min for completion, whereas the same transition requires around 14 min for $G_{58}H_{250}$ vesicles prepared in the presence of 5.0% w/w silica. For $G_{58}H_{250}$ vesicles prepared in the presence of 10% w/w silica, the morphological transition from silica-loaded vesicles to worm clusters plus released silica requires approximately 16 min. For vesicles prepared in the presence of 20 or 30% w/w silica, the morphological transition to perforated vesicles requires around 21 and 23 min, respectively. These observations confirm that the silica nanoparticle loading achieved during the *in situ* PISA synthesis of these diblock copolymer vesicles has a significant influence on the thermal stability of the vesicular morphology.

CONCLUSIONS

The thermally triggered release of silica nanoparticles encapsulated within $G_{58}H_{250}$ diblock copolymer vesicles has

been studied. When silica-loaded vesicles are held at 0 °C for 30 min, TEM images suggest that the fundamental nature of the vesicle dissociation is profoundly affected by the concentration of silica nanoparticles within the lumen. For PISA syntheses conducted in the presence of either no silica or 5.0% w/w silica, the expected vesicle-to-sphere transition is observed. When using 10% w/w silica, the silica-loaded vesicles form aggregated worm clusters on cooling. For 20 or 30% w/w silica, vesicle membranes gradually become perforated, with at least some vesicles remaining intact after 30 min at 0 °C. In all cases, the encapsulated silica nanoparticles are released from the vesicles. Time-resolved SAXS experiments conducted at 0 °C allow the release kinetics to be examined. For empty $G_{58}H_{250}$ vesicles, the vesicles remain intact for 5 min, form worms after 8.75 min, spherical dimers after 10 min, and finally spheres after 12.5 min. Fitting selected SAXS patterns using an appropriate model enables mean aggregation numbers to be calculated for each morphology, with each vesicle dissociating to afford approximately 1750 spheres. For $G_{58}H_{250}$ vesicles prepared in the presence of 30% w/w silica, time-resolved SAXS experiments conducted at 0 °C suggest that most of the vesicles remain intact. However, the disappearance of the silica structure factor present in the original SAXS pattern indicates that the encapsulated silica is released, presumably through perforated vesicle membranes. Data fits for selected SAXS patterns revealed that the scattering length density of the vesicle lumen is reduced monotonically over time for silica-loaded vesicle dispersions held at 0 °C. More detailed analysis revealed that 68% of the encapsulated silica nanoparticles were released within 30 min under these conditions.

ASSOCIATED CONTENT

Supporting Information

The Supporting Information is available free of charge on the ACS Publications website at DOI: 10.1021/acs.macromol.7b00475.

Cartoon depicting the change in dimensions that occur when the $G_{58}H_{250}$ worms are converted into first spherical dimers and then spheres on cooling to 0 °C, variation in X-ray scattering intensity with aging time, TEM images obtained for control experiments whereby silica nanoparticles were added to empty vesicles, characteristic time required to undergo the observed change in morphology against initial silica concentration, and details of SAXS models (PDF)

AUTHOR INFORMATION

Corresponding Authors

*E-mail s.p.arnes@sheffield.ac.uk (S.P.A.).

*E-mail o.mykhaylyk@sheffield.ac.uk (O.O.M.).

ORCID

Matthew J. Derry: 0000-0001-5010-6725

Steven P. Arnes: 0000-0002-8289-6351

Notes

The authors declare no competing financial interest.

ACKNOWLEDGMENTS

We thank Christopher Hill and Svetomir Tzokov at the University of Sheffield Biomedical Science Electron Microscopy Suite for their TEM assistance. The authors are grateful to ESRF (Grenoble, France) for providing SAXS beamtime, and

the personnel of the ID02 stations are thanked for help with these synchrotron experiments. S.P.A. thanks the European Research Council for an ERC Advanced Investigator grant (PISA 320372) to support C.J.M. and also EPSRC for a Platform grant (EP/J007846/1) to support M.J.D. and K.L.T.

REFERENCES

- (1) Nii, T.; Ishii, F. Encapsulation efficiency of water-soluble and insoluble drugs in liposomes prepared by the microencapsulation vesicle method. *Int. J. Pharm.* **2005**, *298*, 198–205.
- (2) Schwartz, L.; Wolf, D.; Markus, A.; Wybraniec, S.; Wiesman, Z. Controlled-Release Systems for the Delivery of Cyromazine into Water Surface. *J. Agric. Food Chem.* **2003**, *51*, 5972–5976.
- (3) Shirley, I. M.; Scher, H. B.; Perrin, R. M.; Wege, P. J.; Rodson, M.; Chen, J.-L.; Rehmknecht, A. W. Delivery of biological performance via micro-encapsulation formulation chemistry. *Pest Manage. Sci.* **2001**, *57*, 129–132.
- (4) Keen, P. H. R.; Slater, N. K. H.; Routh, A. F. Encapsulation of Amylase in Colloidosomes. *Langmuir* **2014**, *30*, 1939–1948.
- (5) Yow, H. N.; Routh, A. F. Release Profiles of Encapsulated Actives from Colloidosomes Sintered for Various Durations. *Langmuir* **2009**, *25*, 159–166.
- (6) Zelisko, P. M.; Aguilar, A. L.; Brook, M. A. Delivery of Both Active Enzyme and Bleach from Water-in-Silicone Oil (D4) Emulsions. *Langmuir* **2007**, *23*, 3620–3625.
- (7) Torchilin, V. P. Recent advances with liposomes as pharmaceutical carriers. *Nat. Rev. Drug Discovery* **2005**, *4*, 145–160.
- (8) Antonietti, M.; Förster, S. Vesicles and liposomes: A self-assembly principle beyond lipids. *Adv. Mater.* **2003**, *15*, 1323–1333.
- (9) Discher, B. M.; Won, Y. Y.; Ege, D. S.; Lee, J. C. M.; Bates, F. S.; Discher, D. E.; Hammer, D. A. Polymersomes: Tough vesicles made from diblock copolymers. *Science* **1999**, *284*, 1143–1146.
- (10) Chécot, F.; Lecommandoux, S.; Gnanou, Y.; Klok, H.-A. Water-Soluble Stimuli-Responsive Vesicles from Peptide-Based Diblock Copolymers. *Angew. Chem., Int. Ed.* **2002**, *41*, 1339–1343.
- (11) Rodríguez-Hernández, J.; Lecommandoux, S. Reversible Inside-Out Micellization of pH-responsive and Water-Soluble Vesicles Based on Polypeptide Diblock Copolymers. *J. Am. Chem. Soc.* **2005**, *127*, 2026–2027.
- (12) Discher, D. E.; Eisenberg, A. Polymer Vesicles. *Science* **2002**, *297*, 967–973.
- (13) Du, J.; Tang, Y.; Lewis, A. L.; Armes, S. P. pH-Sensitive Vesicles Based on a Biocompatible Zwitterionic Diblock Copolymer. *J. Am. Chem. Soc.* **2005**, *127*, 17982–17983.
- (14) Wilson, D. A.; Nolte, R. J. M.; van Hest, J. C. M. Autonomous movement of platinum-loaded stomatocytes. *Nat. Chem.* **2012**, *4*, 268–274.
- (15) Napoli, A.; Valentini, M.; Tirelli, N.; Müller, M.; Hubbell, J. A. Oxidation-responsive polymeric vesicles. *Nat. Mater.* **2004**, *3*, 183–189.
- (16) Tan, J.; Sun, H.; Yu, M.; Sumerlin, B. S.; Zhang, L. Photo-PISA: Shedding Light on Polymerization-Induced Self-Assembly. *ACS Macro Lett.* **2015**, *4*, 1249–1253.
- (17) Photos, P. J.; Bacakova, L.; Discher, B.; Bates, F. S.; Discher, D. E. Polymer vesicles in vivo: correlations with PEG molecular weight. *J. Controlled Release* **2003**, *90*, 323–334.
- (18) Brinkhuis, R. P.; Rutjes, F.; van Hest, J. C. M. Polymeric vesicles in biomedical applications. *Polym. Chem.* **2011**, *2*, 1449–1462.
- (19) Pegoraro, C.; Cecchin, D.; Gracia, L. S.; Warren, N.; Madsen, J.; Armes, S. P.; Lewis, A.; MacNeil, S.; Battaglia, G. Enhanced drug delivery to melanoma cells using PMPC-PDPA polymersomes. *Cancer Lett.* **2013**, *334*, 328–337.
- (20) Deng, Z. Y.; Qian, Y. F.; Yu, Y. Q.; Liu, G. H.; Hu, J. M.; Zhang, G. Y.; Liu, S. Y. Engineering Intracellular Delivery Nanocarriers and Nanoreactors from Oxidation-Responsive Polymersomes via Synchronized Bilayer Cross-Linking and Permeabilizing Inside Live Cells. *J. Am. Chem. Soc.* **2016**, *138*, 10452–10466.
- (21) Yao, C. Z.; Wang, X. R.; Liu, G. H.; Hu, J. M.; Liu, S. Y. Distinct Morphological Transitions of Photoreactive and Thermoresponsive Vesicles for Controlled Release and Nanoreactors. *Macromolecules* **2016**, *49*, 8282–8295.
- (22) Sanson, C.; Schatz, C.; Le Meins, J. F.; Soum, A.; Thevenot, J.; Garanger, E.; Lecommandoux, S. A simple method to achieve high doxorubicin loading in biodegradable polymersomes. *J. Controlled Release* **2010**, *147*, 428–435.
- (23) Ahmed, F.; Pakunlu, R. I.; Srinivas, G.; Brannan, A.; Bates, F.; Klein, M. L.; Minko, T.; Discher, D. E. Shrinkage of a rapidly growing tumor by drug-loaded polymersomes: pH-triggered release through copolymer degradation. *Mol. Pharmaceutics* **2006**, *3*, 340–350.
- (24) Christian, D. A.; Cai, S.; Bowen, D. M.; Kim, Y.; Pajeroski, J. D.; Discher, D. E. Polymersome carriers: From self-assembly to siRNA and protein therapeutics. *Eur. J. Pharm. Biopharm.* **2009**, *71*, 463–474.
- (25) Borchert, U.; Lipprandt, U.; Bilang, M.; Kimpfler, A.; Rank, A.; Peschka-Stüss, R.; Schubert, R.; Lindner, P.; Förster, S. pH-Induced Release from P2VP-PEO Block Copolymer Vesicles. *Langmuir* **2006**, *22*, 5843–5847.
- (26) Huang, J.; Bonduelle, C.; Thévenot, J.; Lecommandoux, S.; Heise, A. Biologically Active Polymersomes from Amphiphilic Glycopeptides. *J. Am. Chem. Soc.* **2012**, *134*, 119–122.
- (27) Lomas, H.; Canton, I.; MacNeil, S.; Du, J.; Armes, S. P.; Ryan, A. J.; Lewis, A. L.; Battaglia, G. Biomimetic pH sensitive polymersomes for efficient DNA encapsulation and delivery. *Adv. Mater.* **2007**, *19*, 4238–4243.
- (28) van Dongen, S. F. M.; Nallani, M.; Cornelissen, J.; Nolte, R. J. M.; van Hest, J. C. M. A Three-Enzyme Cascade Reaction through Positional Assembly of Enzymes in a Polymersome Nanoreactor. *Chem. - Eur. J.* **2009**, *15*, 1107–1114.
- (29) Canton, I.; Massignani, M.; Patikarnmonthon, N.; Chierico, L.; Robertson, J.; Renshaw, S. A.; Warren, N. J.; Madsen, J. P.; Armes, S. P.; Lewis, A. L.; Battaglia, G. Fully synthetic polymer vesicles for intracellular delivery of antibodies in live cells. *FASEB J.* **2013**, *27*, 98–108.
- (30) Lecommandoux, S.; Sandre, O.; Chécot, F.; Rodríguez-Hernández, J.; Perzynski, R. Self-assemblies of magnetic nanoparticles and di-block copolymers: Magnetic micelles and vesicles. *J. Magn. Magn. Mater.* **2006**, *300*, 71–74.
- (31) Lajunen, T.; Viitala, L.; Kontturi, L.-S.; Laaksonen, T.; Liang, H.; Vuorimaa-Laukkanen, E.; Viitala, T.; Le Guével, X.; Yliperttula, M.; Murtomäki, L.; Urtti, A. Light induced cytosolic drug delivery from liposomes with gold nanoparticles. *J. Controlled Release* **2015**, *203*, 85–98.
- (32) Fielding, L. A.; Derry, M. J.; Ladmiral, V.; Rosselgong, J.; Rodrigues, A. M.; Ratcliffe, L. P. D.; Sugihara, S.; Armes, S. P. RAFT dispersion polymerization in non-polar solvents: facile production of block copolymer spheres, worms and vesicles in n-alkanes. *Chem. Sci.* **2013**, *4*, 2081–2087.
- (33) Fielding, L. A.; Lane, J. A.; Derry, M. J.; Mykhaylyk, O. O.; Armes, S. P. Thermo-responsive Diblock Copolymer Worm Gels in Non-polar Solvents. *J. Am. Chem. Soc.* **2014**, *136*, 5790–5798.
- (34) Gonzato, C.; Semsarilar, M.; Jones, E. R.; Li, F.; Krooshof, G. J. P.; Wyman, P.; Mykhaylyk, O. O.; Tuinier, R.; Armes, S. P. Rational Synthesis of Low-Polydispersity Block Copolymer Vesicles in Concentrated Solution via Polymerization-Induced Self-Assembly. *J. Am. Chem. Soc.* **2014**, *136*, 11100–11106.
- (35) Sugihara, S.; Blanazs, A.; Armes, S. P.; Ryan, A. J.; Lewis, A. L. Aqueous Dispersion Polymerization: A New Paradigm for in Situ Block Copolymer Self-Assembly in Concentrated Solution. *J. Am. Chem. Soc.* **2011**, *133*, 15707–15713.
- (36) Blanazs, A.; Madsen, J.; Battaglia, G.; Ryan, A. J.; Armes, S. P. Mechanistic Insights for Block Copolymer Morphologies: How Do Worms Form Vesicles? *J. Am. Chem. Soc.* **2011**, *133*, 16581–16587.
- (37) Blanazs, A.; Ryan, A. J.; Armes, S. P. Predictive Phase Diagrams for RAFT Aqueous Dispersion Polymerization: Effect of Block Copolymer Composition, Molecular Weight, and Copolymer Concentration. *Macromolecules* **2012**, *45*, 5099–5107.

- (38) Warren, N. J.; Armes, S. P. Polymerization-Induced Self-Assembly of Block Copolymer Nano-objects via RAFT Aqueous Dispersion Polymerization. *J. Am. Chem. Soc.* **2014**, *136*, 10174–10185.
- (39) Warren, N. J.; Mykhaylyk, O. O.; Ryan, A. J.; Williams, M.; Doussineau, T.; Dugourd, P.; Antoine, R.; Portale, G.; Armes, S. P. Testing the Vesicular Morphology to Destruction: Birth and Death of Diblock Copolymer Vesicles Prepared via Polymerization-Induced Self-Assembly. *J. Am. Chem. Soc.* **2015**, *137*, 1929–1937.
- (40) Mable, C. J.; Gibson, R. R.; Prevost, S.; McKenzie, B. E.; Mykhaylyk, O. O.; Armes, S. P. Loading of Silica Nanoparticles in Block Copolymer Vesicles during Polymerization-Induced Self-Assembly: Encapsulation Efficiency and Thermally Triggered Release. *J. Am. Chem. Soc.* **2015**, *137*, 16098–16108.
- (41) Rose, S.; PrevotEAU, A.; Elziere, P.; Hourdet, D.; Marcellan, A.; Leibler, L. Nanoparticle solutions as adhesives for gels and biological tissues. *Nature* **2013**, *505*, 382–385.
- (42) Sundararaman, A.; Stephan, T.; Grubbs, R. B. Reversible Restructuring of Aqueous Block Copolymer Assemblies through Stimulus-Induced Changes in Amphiphilicity. *J. Am. Chem. Soc.* **2008**, *130*, 12264–12265.
- (43) Warren, N. J.; Mykhaylyk, O. O.; Mahmood, D.; Ryan, A. J.; Armes, S. P. RAFT Aqueous Dispersion Polymerization Yields Poly(ethylene glycol)-Based Diblock Copolymer Nano-Objects with Predictable Single Phase Morphologies. *J. Am. Chem. Soc.* **2014**, *136*, 1023–1033.
- (44) Lovett, J. R.; Warren, N. J.; Armes, S. P.; Smallridge, M. J.; Cracknell, R. B. Order–Order Morphological Transitions for Dual Stimulus Responsive Diblock Copolymer Vesicles. *Macromolecules* **2016**, *49*, 1016–1025.
- (45) Schumers, J.-M.; Fustin, C.-A.; Gohy, J.-F. Light-Responsive Block Copolymers. *Macromol. Rapid Commun.* **2010**, *31*, 1588–1607.
- (46) Zhang, L.; Eisenberg, A. Morphogenic Effect of Added Ions on Crew-Cut Aggregates of Polystyrene-*b*-poly(acrylic acid) Block Copolymers in Solutions. *Macromolecules* **1996**, *29*, 8805–8815.
- (47) Yu, K.; Eisenberg, A. Bilayer Morphologies of Self-Assembled Crew-Cut Aggregates of Amphiphilic PS-*b*-PEO Diblock Copolymers in Solution. *Macromolecules* **1998**, *31*, 3509–3518.
- (48) Maiti, C.; Banerjee, R.; Maiti, S.; Dhara, D. pH-Induced Vesicle-to-Micelle Transition in Amphiphilic Diblock Copolymer: Investigation by Energy Transfer between in Situ Formed Polymer Embedded Gold Nanoparticles and Fluorescent Dye. *Langmuir* **2015**, *31*, 32–41.
- (49) Scherer, M.; Kappel, C.; Mohr, N.; Fischer, K.; Heller, P.; Forst, R.; Depoix, F.; Bros, M.; Zentel, R. Functionalization of Active Ester-Based Polymersomes for Enhanced Cell Uptake and Stimuli-Responsive Cargo Release. *Biomacromolecules* **2016**, *17*, 3305–3317.
- (50) Ilavsky, J.; Jemian, P. R. Irena: tool suite for modeling and analysis of small-angle scattering. *J. Appl. Crystallogr.* **2009**, *42*, 347–353.
- (51) Derry, M. J.; Fielding, L. A.; Warren, N. J.; Mable, C. J.; Smith, A. J.; Mykhaylyk, O. O.; Armes, S. P. In situ small-angle X-ray scattering studies of sterically-stabilized diblock copolymer nanoparticles formed during polymerization-induced self-assembly in non-polar media. *Chem. Sci.* **2016**, *7*, 5078–5090.
- (52) Fürst, C.; Zhang, P.; Roth, S. V.; Drechsler, M.; Förster, S. Self-assembly of block copolymers via micellar intermediate states into vesicles on time scales from milliseconds to days. *Polymer* **2016**, *107*, 434–444.
- (53) Bang, J.; Jain, S.; Li, Z.; Lodge, T. P.; Pedersen, J. S.; Kesselman, E.; Talmon, Y. Sphere, Cylinder, and Vesicle Nanoaggregates in Poly(styrene-*b*-isoprene) Diblock Copolymer Solutions. *Macromolecules* **2006**, *39*, 1199–1208.
- (54) Madsen, J.; Armes, S. P.; Lewis, A. L. Preparation and Aqueous Solution Properties of New Thermoresponsive Biocompatible ABA Triblock Copolymer Gelators. *Macromolecules* **2006**, *39*, 7455–7457.
- (55) Blanazs, A.; Verber, R.; Mykhaylyk, O. O.; Ryan, A. J.; Heath, J. Z.; Douglas, C. W. I.; Armes, S. P. Sterilizable Gels from Thermo-responsive Block Copolymer Worms. *J. Am. Chem. Soc.* **2012**, *134*, 9741–9748.
- (56) Glatter, O.; Kratky, O. *Small-angle X-ray Scattering*; Academic Press: London, 1982.
- (57) Pedersen, J. S. Form factors of block copolymer micelles with spherical, ellipsoidal and cylindrical cores. *J. Appl. Crystallogr.* **2000**, *33*, 637–640.
- (58) Pedersen, J. S.; Schurtenberger, P. Scattering Functions of Semiflexible Polymers with and without Excluded Volume Effects. *Macromolecules* **1996**, *29*, 7602–7612.
- (59) Cunningham, V. J.; Ratcliffe, L. P. D.; Blanazs, A.; Warren, N. J.; Smith, A. J.; Mykhaylyk, O. O.; Armes, S. P. Tuning the critical gelation temperature of thermo-responsive diblock copolymer worm gels. *Polym. Chem.* **2014**, *5*, 6307–6317.
- (60) Pedersen, J. S.; Gerstenberg, M. C. Scattering Form Factor of Block Copolymer Micelles. *Macromolecules* **1996**, *29*, 1363–1365.
- (61) Hayter, J. B.; Penfold, J. An Analytical Structure Factor for Macroion Solutions. *Mol. Phys.* **1981**, *42*, 109–118.
- (62) Kinning, D. J.; Thomas, E. L. Hard-Sphere Interactions Between Spherical Domains in Diblock Copolymers. *Macromolecules* **1984**, *17*, 1712–1718.
- (63) Dimova, R. Recent developments in the field of bending rigidity measurements on membranes. *Adv. Colloid Interface Sci.* **2014**, *208*, 225–234.